

Elliptic CMB Sky

V.G.Gurzadyan^{1,2}, P. de Bernardis³, G. De Troia³, C.L.Bianco², A.L.Kashin¹, H.Kuloglian¹, S.Masi³, F.Piacentini³, G.Polenta³, G.Yegorian¹

¹ Yerevan Physics Institute, Yerevan, Armenia; ² ICRA, Dipartimento di Fisica, University La Sapienza, Roma, Italy; ³ Dipartimento di Fisica, University La Sapienza, Roma, Italy

Abstract - The ellipticity of the anisotropy spots of the Cosmic Microwave Background measured by the Wilkinson Microwave Anisotropy Probe (WMAP) has been studied. We find an average ellipticity of about 2, confirming with a far larger statistics similar results found first for the COBE-DMR CMB maps, and then for the BOOMERanG CMB maps. There are no preferred directions for the obliquity of the anisotropy spots. The average ellipticity is independent of temperature threshold and is present on scales both smaller and larger than the horizon at the last scattering. The measured ellipticity characteristics are consistent with being the effect of geodesics mixing occurring in an hyperbolic Universe, and can mark the emergence of CMB ellipticity as a new observable constant describing the Universe.

1 Introduction

Several properties of Cosmic Microwave Background (CMB) radiation are known to contain crucial cosmological information. CMB maps are among them. Recently, a significant ellipticity ($\gtrsim 2$) of the anisotropies has been measured [6] in the high signal to noise ratio CMB maps obtained at 150 GHz in the BOOMERanG 1998 experiment [1], [2], [3], [4]. The same effect was shown to exist at scales larger than the horizon at the last scattering epoch [7]. The effect was confirmed when the WMAP [8] data in the same region were used [9], confirming the good consistency of the BOOMERanG and WMAP CMB data [5]. Ellipticity had been reported earlier for the COBE CMB maps [10].

However, the sky region observed by BOOMERanG was small (about 2% of the sky), and hence the statistics of anisotropy areas (spots) was moderate; moreover the COBE map had neither high resolution nor high signal-to-noise ratio. The WMAP first-year maps [8], instead, provide both.

In this paper we analyze the ellipticity in the WMAP W-channel maps of the full sky, and confirm our previous estimates with higher significance, thus firmly establishing the presence of an ellipticity effect.

The analysis of the ellipticity of the areas in CMB maps was motivated by the effect of geodesic mixing [11] (see [12] for a more general discussion) which has to occur in a hyperbolic Universe due to the exponential divergence $L(t)$ of close null geodesics in (3+1)-space at the expansion of the scale factor $a(t)$ from its initial value $a(t_0)$

$$L(t) = L(t_0) \frac{a(t)}{a(t_0)} \exp(h\lambda),$$

where h is the Kolmogorov-Sinai entropy of the geodesic flow and λ is the affine parameter. What we denote as ellipticity is actually the first order approximation of the distortion of the spot. This is due to the exponential instability of the bundle of geodesics, which leads to complex shape anisotropies, with elongated amoeba-like tails. A more informative descriptor of such structures is the Kolmogorov complexity [13].

Therefore, in our analysis, the numerical algorithms did not aim to fit the given spot with an ellipse, but rather to define the effective elongation via the ratio of two semi-axes of the spot. This procedure, described in detail in [6], implies the estimation of Lyapunov exponents of the dynamical system defining the effect, e.g. of the geodesic flow. The information on the Lyapunov exponents and hence on Kolmogorov-Sinai entropy will describe a dynamical system other than the geodesic flow, if being responsible for the observed elongations.

Our analysis of WMAP maps strongly confirmed the existence of a threshold independent mean ellipticity, in the range 2.1 - 2.5 (depending on the size of the areas i.e. on the number of the pixels contained), over the whole interval of temperature thresholds where the areas are well defined, and have reasonable statistics.

We confirmed the existence of the effect for scales smaller and larger than the horizon at recombination. This suggests that the observed effect is not determined by the conditions at the last scattering surface. Note also that for larger (several degrees) areas, the biases of the estimator and of the noise are negligible.

Numerical simulations of the CMB maps in the $\Lambda - CDM$ model fitting the WMAP and Boomerang power spectra led to an average ellipticity around 1.8 [6], while for the once popular CDM model the mean ellipticity is around 1.4 [14].

Our determination of the ellipticity of the CMB sky makes stronger the case that we could be dealing with the effect of geodesic mixing in hyperbolic space. It is known that the low quadrupole detected by WMAP [8] can also be explained by non-zero curvature models, e.g. [15, 16, 17, 18]. However, for a given curvature, an infinite number of topologies is possible. This topological degeneracy excludes the possibility of quantitative comparison of the observational data with a concrete model, since any other model could fit even better. This situation will persist until independent constraints on the topology will be obtained, allowing to remove the degeneracy.

2 Analysis

We used the 94 GHz (3.2mm) maps from WMAP, because these radiometers feature the highest angular resolution (beam size 0.22° FWHM) and also this band is least influenced by the synchrotron radiation from our Galaxy.

We combined the data from the four independent detectors w_i into two independent channels $A = (w_1 + w_2)/2$ and $B = (w_3 + w_4)/2$. We used Healpix [19] maps with $nside=512$ (6.9 arcmin pixel side), excluding all the pixels with galactic latitude $|b| < 20^\circ$. The ellipticity analysis was carried out on the $A + B$ map, and we used the $A - B$ map to investigate the effects of noise (see below).

The algorithms for the definition of the excursion sets have been discussed in detail in previous papers [6, 7]. These algorithms define the hot areas with temperature equal and higher than a given temperature threshold, and the cold areas with temperature equal and lower than the threshold. The center, the semi major and minor axes of the spots were determined by the procedure described in [6]. We tested alternative procedures obtaining consistent results. Since here we are dealing with full-sky maps, we do not project the data on a plane, as was justified in the analysis of small sky patches. We rather perform our analysis on the sphere in Healpix representation.

In Figure 1 we present the average ellipticity (over the number of areas) as a function of the temperature threshold for the $A + B$ map. The computation of the mean ellipticities over the considered temperature intervals yields: 2.50 ± 0.03 , 2.18 ± 0.03 and 2.12 ± 0.05 for areas containing more than 20, 50 and 100 pixels, respectively.

The statistics of the areas (detailed in Figure 2) is one to two order of magnitudes higher than for the BOOMERanG data analysis. However, the results shown in fig.1 are very consistent (compare to [6]), thus confirming

the absence of instrumental / systematic effects.

The error bars shown in fig.1 are statistical only, as they are computed from the standard deviation of the ellipticities of all the areas at a given threshold.

We considered only the threshold interval where the areas are well defined: at small thresholds the areas merge to one-connected region, at higher thresholds the statistics becomes poor. In the considered interval the threshold independence behavior of the ellipticity is evident.

No preferred direction can be defined for the obliquity of the areas, as can be seen from the example in Figure 3. Here we have selected areas containing from 100 up to 500 pixels in the two sky belts at $b = \pm(20^\circ - 40^\circ)$. The threshold is $+200 \mu K$. Such constraints ensure having a sample for which the accuracy of the obliquity estimator is homogenous. Similar results are obtained for other area sizes and thresholds.

We also compared the results found selecting only the northern or the southern hemisphere. No asymmetry of the ellipticity descriptor is found (Figure 4).

We have shown in [6] that for areas containing more than several tens of pixels, the algorithm bias does not exceed 0.1.

Noise in the WMAP maps at 94 GHz is not negligible. The following procedure was used to check its role in our ellipticity estimates. New maps were obtained by adding the difference data $A - B$ (which contain only noise) to different combinations of the w_i data (which contain signal and noise). This procedure effectively changes the signal to noise ratio (S/N) of the map. We analyzed the following maps: $A + B$; $(A' + B)/2$, where $A' = (w_1 + A - B + w_2)/2$; w_1 ; $w_1 + A - B$. The normalized N/S ratio for these maps is (0.5; 0.56; 1.0; 1.71) respectively. We apply to these new maps the same ellipticity analysis used for the original $A + B$ map. The resulting mean ellipticities at a given threshold are plotted in Figure 5. It is evident that there is in fact a noise bias, making the measured ellipticity higher than the true sky ellipticity. This bias is stronger for small spots, which is natural. A naive linear extrapolation to zero noise would suggest that the noise bias in the $A + B$ map is of the order of 0.1. This is an extrapolation, since we do not know the real law describing the noise bias dependence on N/S. However, it is absolutely natural to expect that the extrapolation curves flatten for $N/S \ll 1$. At S/N=4 the extrapolated ellipticities would be 2.3, 2.03, 1.93 for 20, 50 and 100-pixel areas. These can be considered as lower limits. A maximum bias of 0.1 was obtained also with numerical studies of the stability of the semi-axes and of the ellipticity, when distorting only several pixels in areas larger than several tens of pixels (see also [6, 7]).

We did not use simulated maps for the evaluation of the role of the noise. The reason is that for producing simulated maps we start from a model featuring an ellipticity parameter which can be completely different from the real one. The ellipticity estimator can depend on the noise in a way different than in the real case. In this situation either independence or strong dependence of the results on the noise can be misleading. This situation is well known for many-parameter coupled systems. And is similar to the situation we have for the topology, which is also usually neglected in the list of parameters describing the cosmological model. The role of the noise cannot be traced unambiguously unless the maps are created for the given topology.

Therefore, we used the procedure described above to evaluate the role of the noise based on the available real data. Obviously, higher S/N data, e.g. the forthcoming 4-years WMAP maps or the B2K maps, will allow to increase the accuracy of the above evaluation.

3 Conclusions

The spots in the CMB maps of WMAP have an ellipticity around 2. In the previous analysis we could only state the compatibility of the ellipticity with the threshold independence, either due to the low statistics or to the biases. From the present analysis we have a fair, robust establishment of such a behavior. This conclusion is valid for small scales (say 20-pixels), as well as for larger scales, with angular dimensions exceeding one degree.

The measured behavior of the ellipticity suggests a physical interpretation of the data. The temperature threshold independence, the horizon-scale independence, and random orientation are all predicted by geodesic mixing [11]. Moreover, from fig.5 there is an indication that the decrease in the value of the ellipticity when increasing the size of the areas is also intrinsic to the sky. In fact, the lines describing the average ellipticity vs. N/S do not tend to converge at low N/S. This behavior is also predicted by geodesic flows mixing [20] in hyperbolic spaces which, locally, if the space is not compact, behave as Anosov systems [21, 22].

This analysis can mark the emergence of CMB ellipticity as a new observable parameter describing the Universe, which has not been considered in the usual list of parameters defining the concordance cosmological model (see e.g. [8]).

As the power spectrum is degenerate with respect to ellipticity and topology, future studies should aim to break such degeneracies.

References

- [1] de Bernardis P., et al, 2000, *Nature*, 404, 955.
- [2] Netterfield C.B. et al, 2002, *ApJ*, 571, 604
- [3] de Bernardis P., et al, 2002, *ApJ*, 564, 559.
- [4] Ruhl J.E. et al. 2003, *ApJ*, 599, 786.
- [5] de Bernardis P., et al, 2003, *astro-ph/0311396*
- [6] Gurzadyan V.G., Ade P.A.R., de Bernardis P. et al, 2003, *Int.J.Mod.Phys. D*12, 1859.
- [7] Gurzadyan V.G., Ade P.A.R., de Bernardis P. et al, 2005, *Mod.Phys.Lett.*, A20.
- [8] Bennett C.L., et al., 2003, *ApJS* 148, 1.
- [9] Gurzadyan V.G., Ade P.A.R., de Bernardis P. et al, 2003, *Nuovo Cimento*, B118,1101.
- [10] Gurzadyan V.G., Torres S., 1997, *A & A*, 321, 19.
- [11] Gurzadyan V.G., Kocharyan A.A., 1992, *A&A*, 260, 14; *Europhys. Lett.* 1993, 22, 231.
- [12] Penrose R., *The Road to Reality*, Jonathan Cape, London, 2004.
- [13] Gurzadyan V.G., 1999, *Europhys.Lett.*, 46, 114.
- [14] Bond J.R., Efstathiou G., 1987, *MNRAS*, 226, 655.
- [15] Efstathiou G., 2003, *MNRAS*, 343, L95.
- [16] Luminet J.-P. et al, 2003, *Nature*, 425, 593.
- [17] Aurich R., Lustig S., Steiner F., Then H., 2004 *Class. Quant.Grav.* 21, 4901.
- [18] Aurich R., Lustig S., Steiner F., Then H., 2004, *astro-ph/0412407*.
- [19] Górski, K.M., Hivon, E. and Wandelt, B.D., 1998, *astro-ph/9812350*; <http://www.eso.org/kgorski/healpix/>

[20] *Dynamical Systems, Ergodic Theory and Applications*, Ed. Ya.G.Sinai, Springer, 2000.

[21] Anosov D.V., 1967, Comm. Steklov Mathematical Inst., vol.90.

[22] Lockhart C.M., Misra B., Prigogine I. 1982, Phys.Rev. D25, 921.

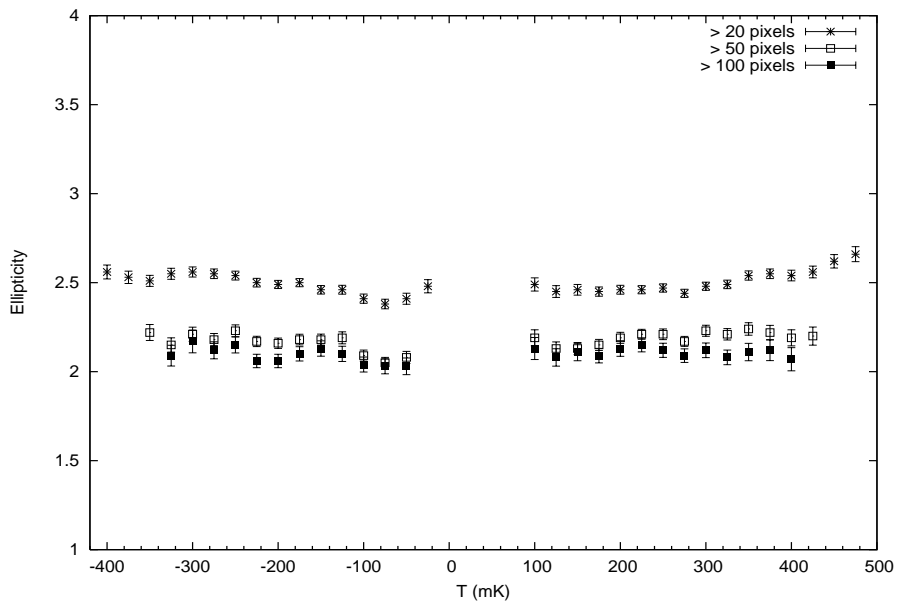


Figure 1: Ellipticity vs temperature threshold (in μK) for the anisotropy areas containing more than 20, 50 and 100 pixels in the 94 GHz sum map A = $(w_1+w_2)/2$ and B = $(w_3+w_4)/2$ of WMAP. The error bars are statistical only.

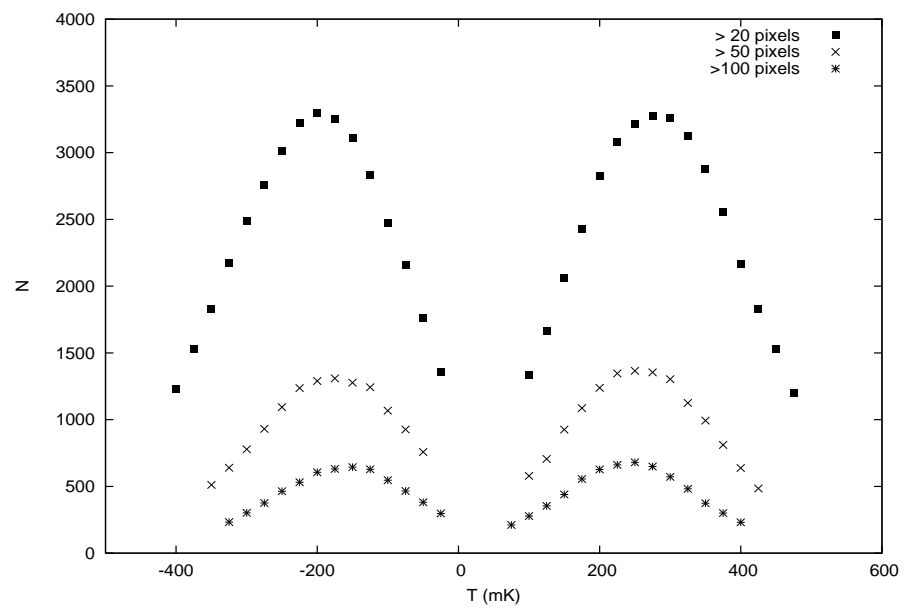


Figure 2: The number of areas containing more than 20, 50 and 100 pixels vs the temperature threshold.

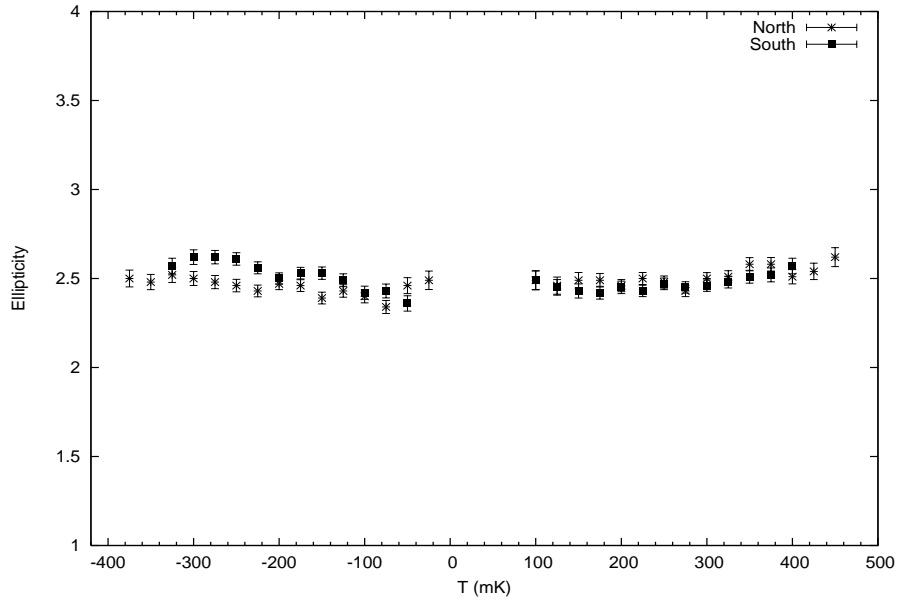


Figure 3: Ellipticity of areas with more than 20-pixels of Southern and Northern Galactic hemispheres.

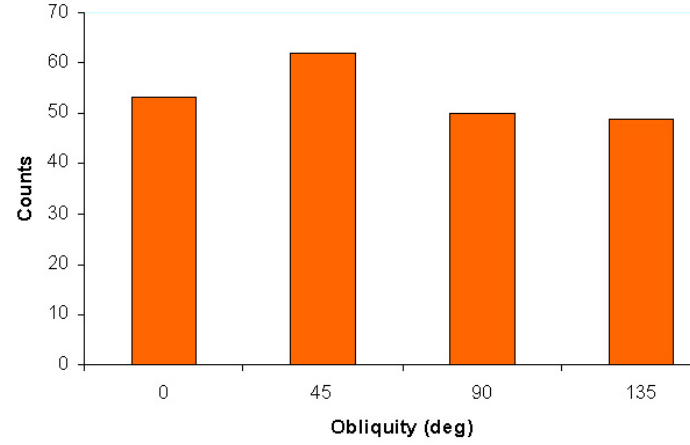


Figure 4: Histogram of obliquities for anisotropy areas containing 100-500 pixels, at temperature threshold $+200 \mu K$ within the two sky belts $\pm(20 - 40)^\circ$.

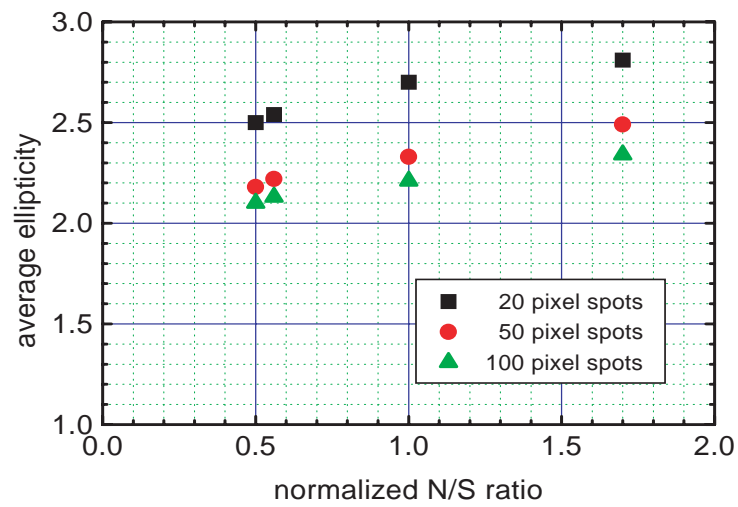


Figure 5: Average ellipticity vs. Noise to Signal ratio. The noise to signal ratio is normalized to be 1 for the map from detector w_1 alone. This plot is used to investigate the noise bias on the ellipticity estimate (see text).